Available online at www.sciencedirect.com
SCIENCE DIRECT
ELSEVIER
Icarus 183 (2006) 479–490
ICARUS
www.elsevier.com/locate/icarus

Cassini RADAR observations of Enceladus, Tethys, Dione, Rhea, Iapetus, Hyperion, and Phoebe

Steven J. Ostro [a,*], Richard D. West [a], Michael A. Janssen [a], Ralph D. Lorenz [b], Howard A. Zebker [c], Gregory J. Black [d], Jonathan I. Lunine [b,e], Lauren C. Wye [c], Rosaly M. Lopes [a], Stephen D. Wall [a], Charles Elachi [a], Laci Roth [a], Scott Hensley [a], Kathleen Kelleher [a], Gary A. Hamilton [a], Yonggyu Gim [a], Yanhua Z. Anderson [a], Rudy A. Boehmer [a], William T.K. Johnson [a],

the Cassini RADAR Team

[a] *Jet Propulsion Laboratory, California Institute of Technology, Mail Stop 300-233, 4800 Oak Grove Drive, Pasadena, CA 91109-8099, USA*
[b] *Lunar and Planetary Laboratory, University of Arizona, Tucson, AZ 85721-0092, USA*
[c] *Department of Electrical Engineering, Stanford University, Stanford, CA 94305-9515, USA*
[d] *Department of Astronomy, University of Virginia, P.O. Box 3818, Charlottesville, VA 22903, USA*
[e] *INAF-IFSI ARTOV, Via del Fosso del Cavaliere 100, 00133 Rome, Italy*

Received 19 November 2005; revised 24 February 2006

Available online 27 April 2006

Abstract

Cassini 2.2-cm radar and radiometric observations of seven of Saturn's icy satellites yield properties that apparently are dominated by subsurface volume scattering and are similar to those of the icy Galilean satellites. Average radar albedos decrease in the order Enceladus/Tethys, Hyperion, Rhea, Dione, Iapetus, and Phoebe. This sequence most likely corresponds to increasing contamination of near-surface water ice, which is intrinsically very transparent at radio wavelengths. Plausible candidates for contaminants include ammonia, silicates, metallic oxides, and polar organics (ranging from nitriles like HCN to complex tholins). There is correlation of our targets' radar and optical albedos, probably due to variations in the concentration of optically dark contaminants in near-surface water ice and the resulting variable attenuation of the high-order multiple scattering responsible for high radar albedos. Our highest radar albedos, for Enceladus and Tethys, probably require that at least the uppermost one to several decimeters of the surface be extremely clean water ice regolith that is structurally complex (i.e., mature) enough for there to be high-order multiple scattering within it. At the other extreme, Phoebe has an asteroidal radar reflectivity that may be due to a combination of single and volume scattering. Iapetus' 2.2-cm radar albedo is dramatically higher on the optically bright trailing side than the optically dark leading side, whereas 13-cm results reported by Black et al. [Black, G.J., Campbell, D.B., Carter, L.M., Ostro, S.J., 2004. Science 304, 553] show hardly any hemispheric asymmetry and give a mean radar reflectivity several times lower than the reflectivity measured at 2.2 cm. These Iapetus results are understandable if ammonia is much less abundant on both sides within the upper one to several decimeters than at greater depths, and if the leading side's optically dark contaminant is present to depths of at least one to several decimeters. As argued by Lanzerotti et al. [Lanzerotti, L.J., Brown, W.L., Marcantonio, K.J., Johnson, R.E., 1984. Nature 312, 139–140], a combination of ion erosion and micrometeoroid gardening may have depleted ammonia from the surfaces of Saturn's icy satellites. Given the hypersensitivity of water ice's absorption length to ammonia concentration, an increase in ammonia with depth could allow efficient 2.2-cm scattering from within the top one to several decimeters while attenuating 13-cm echoes, which would require a six-fold thicker scattering layer. If so, we would expect each of the icy satellites' average radar albedos to be higher at 2.2 cm than at 13 cm, as is the case so far with Rhea [Black, G., Campbell, D., 2004. Bull. Am. Astron. Soc. 36, 1123] as well as Iapetus.

Keywords: Satellites of Saturn; Surfaces, satellite; Radar

* Corresponding author. Fax: +1 (818) 354 9476.
E-mail address: ostro@reason.jpl.nasa.gov (S.J. Ostro).

0019-1035/$ – see front matter
doi:10.1016/j.icarus.2006.02.019

1. Introduction

The Cassini mission includes 34 investigations of Saturn's icy satellites by the 2.2-cm-wavelength (13.8-GHz) RADAR instrument, operating both as a scatterometric radar and a passive radiometer. These measurements are sensitive to near-surface electrical properties and structure at scales about six times smaller than the only groundbased radar wavelength available to study the satellites (13 cm) and 22 times longer than the millimeter wavelengths at the limit of Cassini's Composite Infrared Spectrometer (CIRS). Here we present Cassini's first radar results for seven of the satellites.

2. Radar astronomical terminology and context

Most groundbased radar astronomy during the past few decades consists of Arecibo 13-cm observations and Goldstone 3.5-cm observations, almost always using transmission of a circularly polarized signal and reception of echoes in the same circular (SC) and opposite circular (OC) polarizations. Very rarely, the transmission has been linearly polarized, with reception in the same linear (SL) and orthogonal linear (OL) polarizations.

A radar target's most basic disk-integrated property is its radar albedo, defined as its radar cross section divided by its projected area. The radar cross section is the projected area of a perfectly reflective, isotropic scatterer which, if observed at the target's distance from the radar and using the same transmitted and received polarizations, would return the observed echo power. The total-power radar albedo is the sum of the albedos in two orthogonal polarizations:

$$\mathrm{TP} = \mathrm{SL} + \mathrm{OL} = \mathrm{SC} + \mathrm{OC}. \tag{1}$$

For a smooth, homogeneous, spherical target, single backreflections would be entirely OC when the transmission is circularly polarized or entirely SL when the transmission is linearly polarized, so the polarization ratios SC/OC and OL/SL would equal zero. The OC and SL radar albedos would equal the surface's Fresnel normal-incidence reflection coefficient R, which for most materials of planetary interest is predicted fairly accurately by simple empirical functions of bulk density d (g cm^{-3}), such as

$$R(d) = \left\{\left[\exp(d/3.2) - 1\right]/\left[\exp(d/3.2) + 1\right]\right\}^2 \tag{2}$$

from Garvin et al. (1985) and

$$R(d) = 0.12d - 0.13 \tag{3}$$

from Ostro et al. (1985).

Echoes from rough interfaces (with Gaussian radii of curvature near the wavelength) or due to multiple reflections or refractions would produce SC or OL power. For example, randomly oriented dipoles would give SC/OC = 1 and OL/SL = 1/3 (Long, 1965). Echoes from the Moon, the inner planets, and most asteroids have SC/OC $\leqslant 0.3$, because so-called quasi-specularly scattered echo from the "smooth component" of the surface is much stronger than diffusely scattered power from surface and subsurface roughness. These *rocky* objects' total-power radar albedos are typically of order 0.1, as predicted by the above laws for backreflection from silicate regoliths with $d \sim 2$. From Kirchoff's law, the emissivity of a surface is complementary to its reflectivity (see the discussion in Section 4 of Pettengill et al., 1988); hence emissivities of about 0.9 are common for those objects.

The icy Galilean satellites (Table 2) are radically different, with SC/OC > 1, total-power albedos between ∼0.5 and ∼2.5, and emissivities much lower than those measured for rocky objects. Their echoes arise from volume scattering within regoliths that are predominantly water ice, whose extreme radio-wavelength transparency permits subsurface multiple scattering that otherwise would be attenuated.

We stress that extremely clean ice is an insufficient condition for anomalously large radar albedos and circular polarization ratios, which arise from multiple scattering within a random, disordered medium whose intrinsic microwave absorption is very low. Thus perfectly clean ice that is structurally homogeneous (constant-density) would not give anomalous echoes. The regoliths on Solar System objects are structurally very heterogeneous, with complex density variations from the distribution of particle sizes and shapes produced by impacts by projectiles with diverse sizes and impact energies (Veverka et al., 1986). We expect that the uppermost few meters of Saturn's icy satellite regoliths are basically similar to those of the icy Galilean satellites or the Moon's in terms of particle-size distributions, porosity and density as functions of depth, and lateral/vertical heterogeneity. It is the *combination* of complex density variations and radio transparency that gives icy regoliths their exotic radar properties (e.g., MacKintosh and John, 1989; Hapke, 1989; Peters, 1992; Black, 1997).

3. Cassini RADAR instrument and techniques

The Cassini RADAR was designed primarily for synthetic aperture imaging of Titan during close flybys, but the instrument has enough flexibility for a broad variety of radar measurements (Elachi et al., 2005a, 2005b). It includes a radiometer channel that observes passive emission simultaneously with, or separately from, the active measurements. The icy satellite observations are distinguished by relatively long distances to the target: from 50,000 km out to 420,000 km, vs about 1000 km for some Titan flybys. The corresponding target angular sizes vary from half to twice the 0.373°, one-way, half-power beamwidth of Cassini's 4-m high-gain antenna. The radar uses the antenna to transmit 46 W in bursts of continuous-wave pulses. Spacecraft power constraints limit the radar to a 7% transmit duty cycle, so the actual data integration time is much less than the typical 5 to 10 min of a single observing sequence.

The receiver operates with a relatively high noise temperature of about 900 K, and the received echo power is well below the noise floor. To overcome the low instantaneous signal-to-noise ratio (SNR), the radar stares at the target body while recording echoes as real offset video voltage samples, which are Fourier transformed to produce echo power spectra. The latter are summed to maximize the SNR.

The received echo power is spread out in Doppler frequency because of the target's apparent rotation, which is the sum of

Table 1
Observations, results, and accessory information

Satellite	Obsn	Date	W. long. (deg)	Lat. (deg)	Beam/ diam.	Range (km)
Phoebe	PH In	2004 Jun 11	246	−22	2.82	92,525
Phoebe	PH Out	2004 Jun 11	328	+27	1.76	58,230
Iapetus "L"	IA-B In	2004 Dec 31	66	+39	0.68	150,823
Iapetus "T"	IA-C Out	2005 Jan 1	296	+46	0.91	202,360
Enceladus	EN 3	2005 Feb 17	360	0	2.14	165,480
Enceladus	EN 4	2005 Mar 9	70	−13	1.08	83,059
Rhea	RH 11	2005 Jul 14	62	−74	0.82	193,603
Tethys	TE 15	2005 Sep 24	207	1	0.74	120,908
Hyperion	HY 15	2005 Sep 26	172	+58	2.08	85,911
Dione	DI 16	2005 Oct 11	14	0	0.64	111,088

Satellite	Obsn	Assumed radius	Scat. law exponent, n	SL albedo	$T_{\rm disk}$ (K)
Phoebe	PH In	105.8	0.9 ± 0.2	0.17 ± 0.02	93.2 ± 3.6
Phoebe	PH Out	107.0	1.2 ± 0.5	0.18 ± 0.01	75.0 ± 3.5
Iapetus "L"	IA-B In	718.0	1.1 ± 0.1	0.31 ± 0.02	73.0 ± 2.2
Iapetus "T"	IA-C Out	718.0	1.3 ± 0.6	0.57 ± 0.02	57.1 ± 1.7
Enceladus	EN 3	249.4	2.0 ± 0.9	1.53 ± 0.01	36.2 ± 3.2
Enceladus	EN 4	249.4	1.8 ± 0.8	1.67 ± 0.12	30.7 ± 1.1
Rhea	RH 11	764.0	1.7 ± 0.8	1.06 ± 0.03	46.5 ± 1.5
Tethys	TE 15	529.9	1.8 ± 0.8	1.54 ± 0.03	32.0 ± 1.0
Hyperion	HY 15	133.7		>1.3	~ 63
Dione	DI 16	560.0	1.6 ± 0.7	0.94 ± 0.19	50.8 ± 1.7

Satellite	Distance from Saturn ($R_{\rm sat}$)	Ave. SL albedo	Ave. $T_{\rm disk}$ (K)	Optical properties				$T_{\rm eq}$ (K)	Ave. emissivity
				Filter	Geometric albedo	Phase integral	Bond albedo		
Enceladus	3.94	1.60	33.4	Vgr	1.00	0.85	0.85	56.9	0.59
Tethys	4.88	1.54	32.0	Vgr	0.80	0.75	0.60	72.7	0.44
Dione	6.26	0.94	50.8	Vgr	0.55	0.80	0.45	78.7	0.65
Rhea	8.74	1.06	46.5	Vgr	0.65	0.70	0.45	78.7	0.59
Iapetus "L"	59.0	0.31	73.0	V	0.08	0.775	0.062	89.9	0.81
Iapetus "T"	59.0	0.57	57.1	V	0.40	0.775	0.31	83.3	0.69
Phoebe	214.7	0.18	84.1	V	0.06	0.775	0.0046	91.3	0.92

Note. The listed standard errors in the scattering law exponent n, the SL radar albedo, and radiometric brightness temperature $T_{\rm disk}$ incorporate statistical and calibration uncertainties. For the SL albedo, the standard errors are relative uncertainties; the overall one-sigma uncertainty in our absolute calibration of radar cross sections is about 10%. For Iapetus, "L" and "T" flag observations of the leading and trailing sides. Hyperion's elongated shape makes it a special case; our analysis of the data is incomplete and our results are preliminary. $T_{\rm disk}$ is the measured average 2.2-cm brightness temperature over a disk of the assumed radius. The values for geometric albedo and phase integral are from Tables I and II of Morrison et al. (1986), for either the Voyager clear filter (0.47 μm) or a V filter. The Bond albedo is the product of the geometric albedo and the phase integral. Lacking values for the phase integrals of Phoebe and Iapetus, we have assumed the other satellites' average value. We use the Bond albedo $A_{\rm Bond}$ to calculate the isothermal equilibrium temperature, $T_{\rm eq} = 91.4(1 - A_{\rm Bond})^{1/4}$, a first approximation to the surface's physical temperature. The values for emissivity equal $T_{\rm disk}/T_{\rm eq}$.

the target's intrinsic spin and the changing direction of the spacecraft-target vector. For the icy satellites, echo bandwidths range from a few hundred Hz to several kHz. The pulsed transmit waveform introduces grating lobes spaced at the pulse-repetition frequency (PRF), but by setting the PRF to a frequency higher than the target's echo bandwidth, we can keep the echo spectrum from overlapping the grating lobes.

4. Overview of radar and radiometric results

Table 1 lists parameters of our observations, and Fig. 1 shows our echo spectra. None of the spectra, and none of the groundbased echo spectra from any of our targets or the icy Galilean satellites, show any hint of the specular (narrowband) scattering expected if the echoes were dominated by single backreflections from surface elements that are large and smooth at scales near the wavelength. Rather, the spectral shapes are broad, indicating diffuse scattering from structural complexity at some scale(s) comparable to the wavelength or larger. Diffuse scattering is commonly described by a scattering law of the form $d\sigma/dA \sim \cos^n \theta$, where σ is radar cross section, A is surface area, θ is incidence angle, and n is typically about 1.5. A uniformly bright scatterer, like the full moon at optical wavelengths, would have $n = 1$, and a Lambert scatterer would have $n = 2$. Estimates of n from groundbased observations of Europa, Ganymede, and Callisto at 3.5 cm, the closest available wavelength to Cassini's, have respective means and r.m.s. dispersions of 1.7 ± 0.4, 1.3 ± 0.2, and 1.4 ± 0.3 (Ostro et al., 1992).

Table 2
Radar and radiometric properties of Europa, Ganymede, and Callisto

Radar properties		13-cm	3.5-cm	70-cm
Europa	TP	2.60 ± 0.22	2.31 ± 0.36	$\leqslant 0.95 \pm 0.36$
	OC	1.03 ± 0.08	0.91 ± 0.13	
	SC	1.58 ± 0.14	1.40 ± 0.23	
	OL	0.83 ± 0.21		
	SL	1.77 ± 0.44		
	SC/OC	1.53 ± 0.03	1.43 ± 0.24	1.7 ± 0.4
	OL/SL	0.47 ± 0.07		
	(SC/OC)/(OL/SL)	$3.26 + 0.57, -0.43$		
Ganymede	TP	1.39 ± 0.14	1.55 ± 0.20	$0.62 \pm \sim 0.2$
	OC	0.57 ± 0.06	0.65 ± 0.10	
	SC	0.82 ± 0.09	0.90 ± 0.10	
	OL	0.48 ± 0.11		
	SL	1.03 ± 0.24		
	SC/OC	1.43 ± 0.06	1.40 ± 0.10	1.44 ± 0.19
	OL/SL	0.47 ± 0.08		
	(SC/OC)/(OL/SL)	$3.04 + 0.64, -0.46$		
Callisto	TP	0.69 ± 0.06	0.72 ± 0.06	$\leqslant 0.18 \pm 0.06$
	OC	0.32 ± 0.03	0.32 ± 0.02	
	SC	0.37 ± 0.03	0.40 ± 0.04	
	OL	0.23 ± 0.06		
	SL	0.41 ± 0.11		
	SC/OC	1.17 ± 0.04	1.22 ± 0.08	> 2.2
	OL/SL	0.55 ± 0.10		
	(SC/OC)/(OL/SL)	$2.13 + 0.48, -0.33$		

Radiometric properties		2-cm	6-cm
Europa	Disk temp. (K)	47 ± 10	44 ± 10
	Eq. temp. (K)	97	97
	Emissivity	0.48	0.45
Ganymede	Disk temp. (K)	67 ± 6	55 ± 6
	Eq. temp. (K)	107	107
	Emissivity	0.63	0.51
Callisto	Disk temp. (K)	92 ± 9	105 ± 7
	Eq. temp. (K)	117	117
	Emissivity	0.79	0.90

Note. 3.5- and 13-cm radar results are from Ostro et al. (1992) except for the linear polarization results, which are from Ostro et al. (1980). 70-cm results are from Black et al. (2001a). Radiometric results are from de Pater et al. (1984). We use Fieller's Theorem (Finney, 1964) to set upper and lower one-sigma limits on the (SC/OC)/(OL/SL) ratio.

If a radar target is illuminated by a uniform antenna beam (that is, if the antenna gain is constant across the disk), then it is a simple matter to use the appropriate "radar equation" to convert the measured echo power to a radar cross section (e.g., Ostro, 1993). For our measurements, with the antenna beamwidth within a factor of two of the target's angular width, the gain varies across the target's disk, usually significantly. The data reduction yields an estimate of echo power which is a sum of contributions from different parts of the surface, with each contribution weighted by the two-way gain. However, the distribution of echo power as a function of location on the target disk is not known a priori. Thus we do not know how much the echo power from any given surface element has been "amplified" by the antenna gain, and to estimate a radar albedo from our data we must make an assumption about the homogeneity and angular dependence of the surface's radar scattering. Here, for the purpose of obtaining a radar albedo estimate from each observation, we have assumed spherical targets with uniform, azimuthally isotropic, $\cos^n \theta$ scattering laws, and have used least squares to estimate the scattering law exponent n from each echo power spectrum.

The radiometer channel observes the thermal emission at essentially the same wavelength and with the same aperture. Because the satellite's disk is at best barely resolved, we report only the total emission, expressed as the disk-averaged brightness temperature

$$T_{\text{disk}} = (1/\Omega_{\text{disk}}) \int T_{\text{B}}\, \mathrm{d}\Omega, \tag{4}$$

where Ω_{disk} is the disk solid angle and T_{B} is the brightness temperature of each element of solid angle $\mathrm{d}\Omega$. The observations consisted of raster scans over a rectangular area approximately two degrees on a side, with the raster spacing less than one-half of the 0.37-deg beamwidth of the radiometer. Such raster scans were performed just before or just after each scatterometry measurement. The measured signal can be represented as the convolution of the beam, whose shape is well known, with

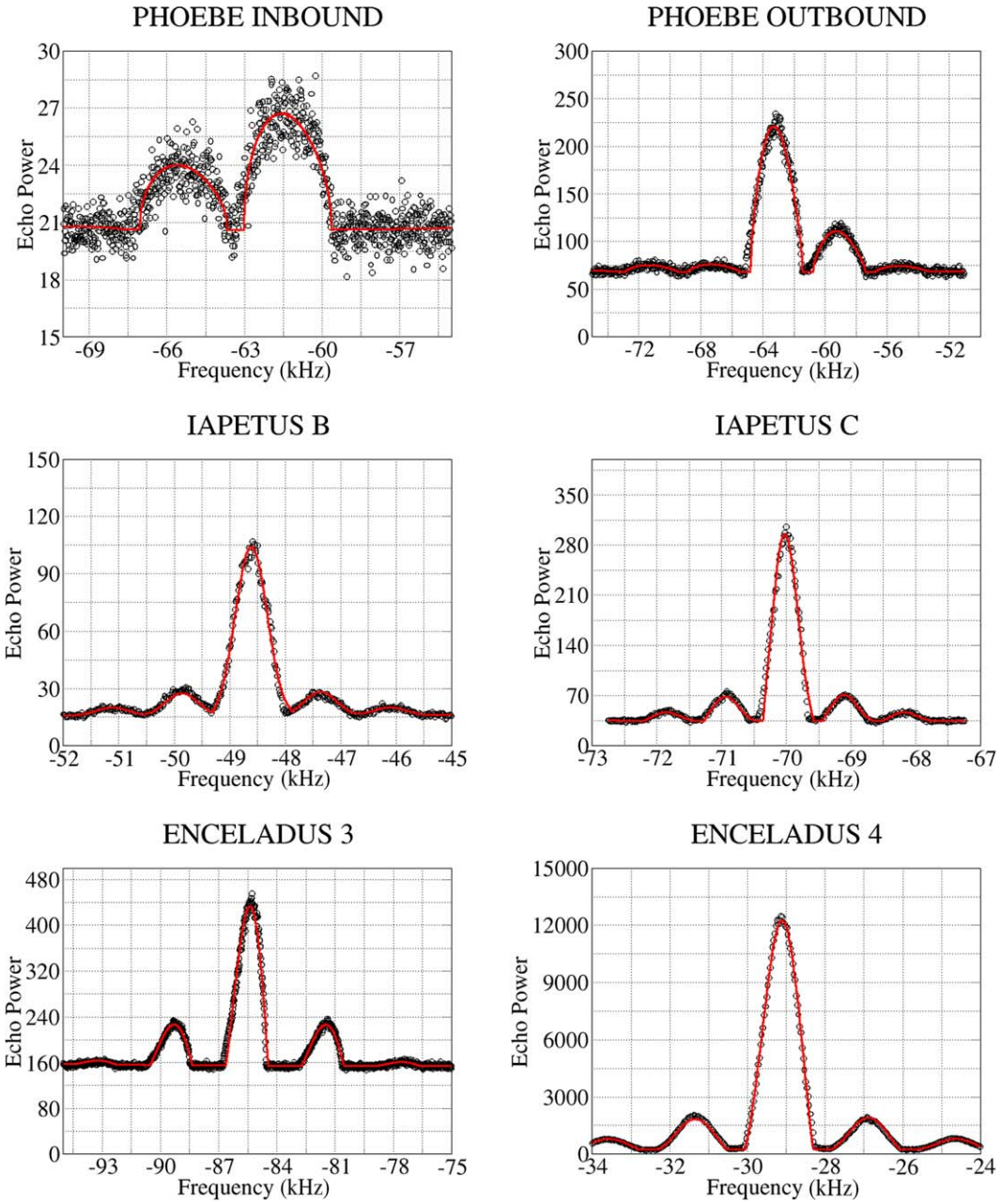

Fig. 1. Cassini 2.2-cm radar echo power spectra (symbols) and model fits (red lines). Relative echo power per 15-Hz resolution cell is plotted vs relative Doppler frequency. The pulsed transmit waveform introduces grating lobes spaced at the pulse-repetition frequency (PRF), but by setting the PRF to a frequency higher than the target's echo bandwidth, we can keep the center of the echo spectrum equidistant from the grating lobes. This was inadvertently not done for the Phoebe observations, causing the spectra to be split. Our modeling of the Hyperion spectrum is in progress. See text and Table 1.

the source brightness distribution, and is fully sampled by the raster scan. The total power of such a convolved signal integrated over solid angle is equal to the total emission from the disk, independent of assumptions about the source brightness distribution or radiometer beam pattern. The precision of each determination was sufficiently high that the net uncertainty is dominated by that of the radiometer's absolute calibration, which was obtained by comparing our measurements of Saturn's radiometric emission in April 2005 to 2.0-cm observations by the Very Large Array (VLA) in previous years as referenced to the radioastronomical flux scale given by Baars et al. (1977); see Janssen et al. (2005).

4.1. Radar albedos

The Cassini radar obtains echoes just in the SL polarization. Table 1 lists our estimates of n and corresponding estimates of the SL albedo. Groundbased estimates of SL albedos are available at various wavelengths for the Moon (∼0.07) and at 13-cm for Europa (1.77), Ganymede (1.03), and Callisto (0.41); see Table 2. Even Phoebe, our dimmest radar target, is more than twice as radar bright as the Moon, and the distribution of the rest of our targets' average SL albedos is comparable to that for the icy Galilean satellites.

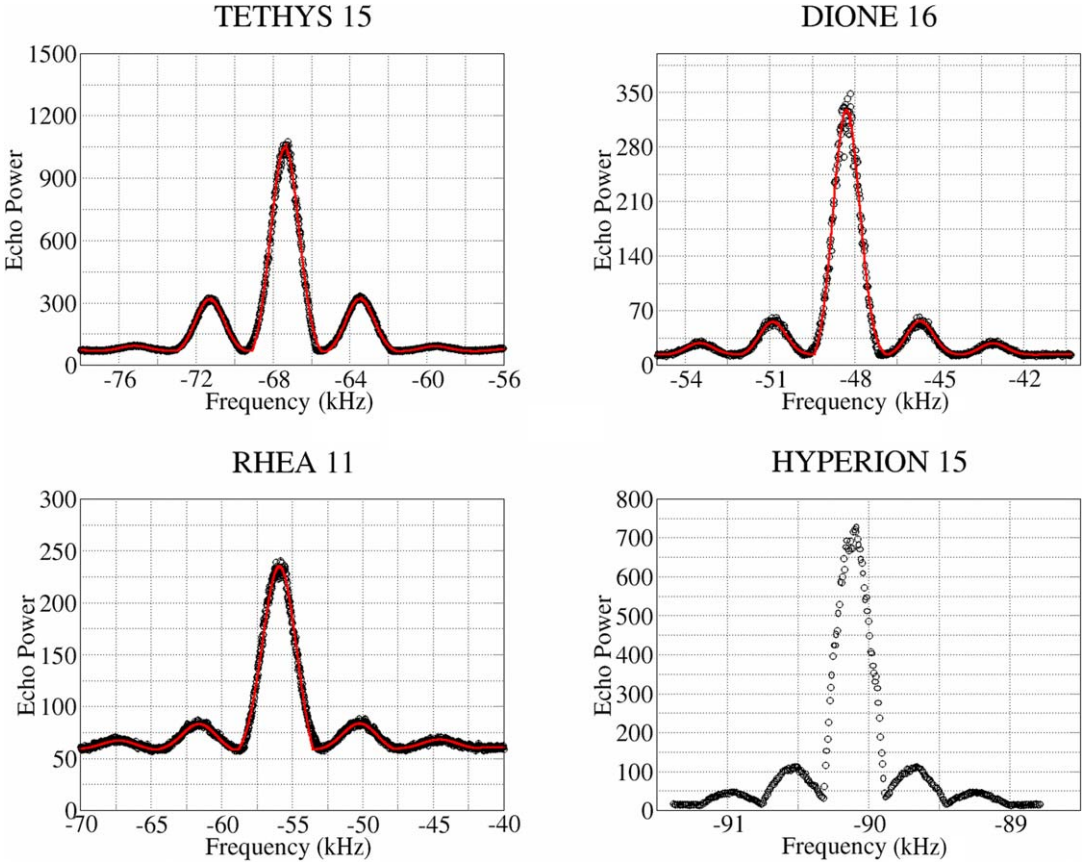

Fig. 1. (*continued*)

To be able to discuss our results within the broader context of all available groundbased radar results for icy satellites, we must constrain our target's total-power (TP) albedos. This is tantamount to constraining their OL/SL ratios. For radar observations of Solar System bodies, OL/SL $\leqslant 0.7$ (Ostro et al., 1980; Ostro, 1993), so TP can be assumed to be between SL and 1.7 SL. The only relevant targets for which linear polarization ratios have been made are the icy Galilean satellites, whose 13-cm weighted-mean radar properties are given in Table 2. Those objects' 13-cm SC/OC ratios are between 1.1 and 1.6, their OL/SL ratios are each about one-half, and one-sigma bounds on their (SC/OC)/(OL/SL) ratios fall between 1.8 and 3.8 (straddling the value, 3, of that ratio for echoes from randomly oriented dipoles, as noted above). There is correlation between (SC/OC)/(OL/SL) and (SC/OC), as sketched in Fig. 2:

$$(\mathrm{SC/OC})/(\mathrm{OL/SL}) = -1.61 + 3.21 \times (\mathrm{SC/OC}). \quad (5)$$

Given the similarity of our targets' radar albedos and angular scattering laws to those of the Galilean satellites, their SC/OC and OL/SL ratios may also be similar. Accordingly, we have used the above relation to estimate our targets' *nominal* TP albedos as a function of SC/OC within the interval $1.1 \leqslant \mathrm{SC/OC} \leqslant 1.6$; corresponding nominal values of the linear polarization ratio satisfy $0.57 \geqslant \mathrm{OL/SL} \geqslant 0.45$. Fig. 3 plots the results along with available groundbased estimates of icy satellites' TP albedos and circular polarization ratios. The uncertainties in our targets' TP albedos are comparable to the vertical extents of the curves in Fig. 3.

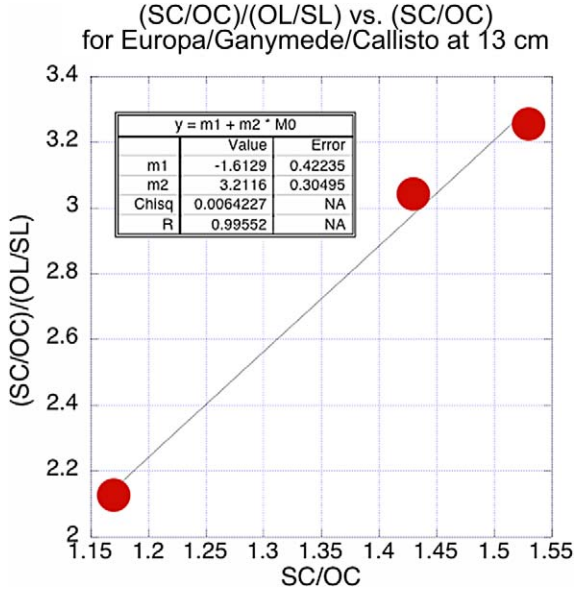

Fig. 2. The (SC/OC)/(OL/SL) ratio vs SC/OC for 13-cm observations of the icy Galilean satellites and a linear fit. See text and Table 2.

Our targets' radar albedos span an order of magnitude and are correlated with the satellites' optical albedos (Table 1 and Fig. 4). In terms of *average* TP albedo, Enceladus and Tethys at 2.2 cm resemble Europa at 3.5 and 13 cm, Rhea and Dione

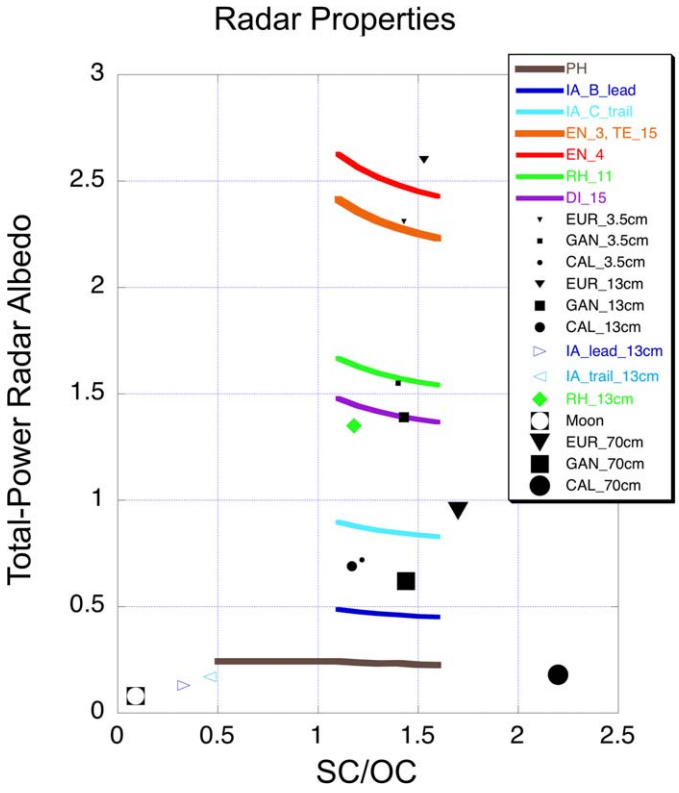

Fig. 3. Total-power (TP) radar albedos from Cassini 2.2-cm observations (curves) and from groundbased measurements (symbols). As explained in the text, Cassini measured SL albedos, and the TP = SL + OL albedos depend on the unknown OL/SL ratio. For the icy Galilean satellites, the linear and circular polarization properties are related; here we assume that the correlation shown in Fig. 2 applies, and we plot TP as a function of SC/OC within the range of that ratio encompassing the icy Galilean satellite values. Phoebe's low albedo allows lower SC/OC, so its curve is extended horizontally (that is, not using Eq. (5)) leftward to SC/OC = 0.5, as measured for Iapetus at 13 cm. The uncertainty in Cassini TP albedos is comparable to the vertical extent of the curves.

at 2.2 cm (and Rhea at 13 cm; Black and Campbell, 2004) resemble Ganymede at 3.5 and 13 cm, and Iapetus at 2.2 cm resembles Callisto at 3.5 and 13 cm.

Modeling of icy Galilean satellite echoes suggests that penetration to a few meters is adequate for volume scattering to produce the highest 13-cm TP albedos (Black et al., 2001b). Therefore, penetration to about half a meter should be adequate to produce our largest 2.2-cm albedos. Depending on the regolith structure and electrical properties, a decimeter might suffice for the lower albedos.

4.2. Radiometric emissivities

As with the icy Galilean satellites, our targets' radar properties indicate that subsurface volume scattering dominates most of our echoes. This conclusion is supported by the strong anticorrelation between our targets' radar albedos and passive radiometric disk brightness temperatures. Our measurements of $T_{\rm disk}$ correspond to the emissivity multiplied by the mean physical temperature at the effective emission depth for 2.2 cm wavelength radiation. A first approximation to that physical temperature is the isothermal equilibrium temperature, $T_{\rm eq} = 91.4(1 - A_{\rm Bond})^{1/4}$, where $A_{\rm Bond}$ is the Bond albedo and 91.4 K is the equilibrium temperature for a grey body at Saturn's distance from the Sun during our observations (e.g., de Pater and Lissauer, 2001, pp. 48–49).

For a spherical target with a perfectly smooth, homogeneous, porous icy surface (a simple dielectric interface), the SL = TP radar albedo would be about 0.1 and the emissivity would be about 0.9, so that one would expect $T_{\rm disk}$ slightly lower than the physical temperature. However, enhanced reflectivity due to volume scattering will decrease the emissivities and lower the disk temperatures. As articulated by Pettengill et al. (1992), "we can think of the effects of decreasing emissivity as actually the result of increasing surface albedo, where the decreasing emitted energy is replaced by the increased efficiency of scattering 'cold sky' towards the observer." The decreasing emissivities moving inward from Phoebe to Enceladus (Table 1) are consistent with progressively increasing volume scattering and the higher observed radar albedos (Fig. 5). Note in particular the consistent anticorrelation between Iapetus' disk temperature and radar albedo for our leading- and trailing-side flybys.

4.3. What about Phoebe?

Phoebe, our dimmest radar target, has an average TP radar albedo between 0.17 and 0.31, an interval that falls in the brighter half of the 13-cm distribution for main belt asteroids (Magri et al., 1999), whose generally low SC/OC ratios (∼0.2) imply dominance of the echoes by single backreflections from smooth surface elements. If such reflections were entirely responsible for Phoebe's echo, the high SL albedo would require a surface bulk density greater than 2.0 g cm^{-3} (Eqs. (2) and (3)), which is precluded by Phoebe's mean internal bulk density of 1.63 g cm^{-3} (Porco et al., 2005). But that apparent contradiction would vanish if only a few tens of percent of the SL echo power arose from such reflections from a smooth surface component, with the balance coming from small-scale surface roughness or from volume scattering. Thus, whereas Phoebe's disk temperature indicates a relatively high emissivity and hence moderate volume scattering, its radar albedo allows a contribution from surface scattering. That is, part of the echo might be due to single backscattering from surface elements that are smooth at 2.2 cm but with large slopes with respect to the mean surface, and part might come from volume scattering in a regolith whose water ice is more contaminated with non-H_2O material than on our other targets. We are unable to ascertain the relative contributions of these putative echo components, but we suspect that if there were a specular component, Phoebe's rather dramatic topography would have produced some glints in the spectra. None are evident.

One way or another, contaminants are probably responsible for Phoebe's relative radar darkness. Radar detected comet nuclei are several times darker still (Harmon et al., 2004), perhaps because of unusually high dust-to-ice ratios (e.g., Küppers et al., 2005).

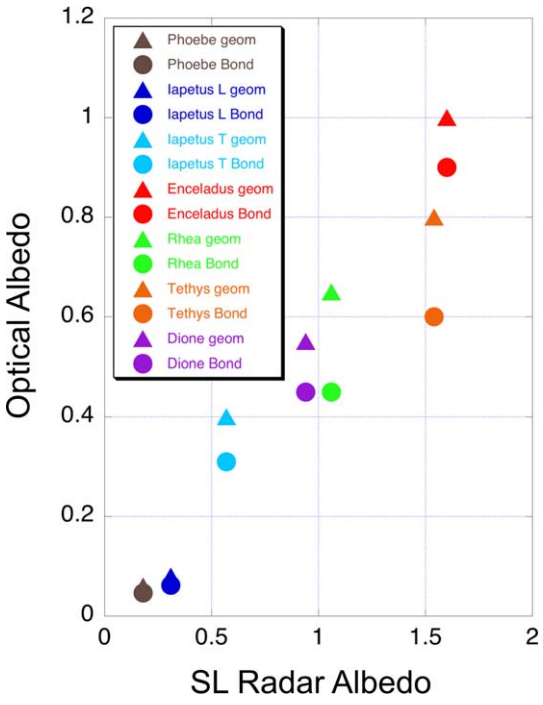

Fig. 4. Optical geometric albedo (triangles) and Bond albedo (circles) plotted vs Cassini 2.2-cm SL radar albedo (Table 1).

5. Effects of contaminants on radar and optical albedos

The correlation of our targets' radar and optical albedos, also seen for groundbased radar observations of the icy Galilean satellites, is most easily understood as involving variations in the concentration of optically dark contaminants in near-surface water ice and the consequent variable attenuation of the high-order multiple scattering responsible for high radar albedos. Plausible candidates for contaminants causing variations in radar albedo include silicates, metal oxides, and polar organics such as nitriles like HCN and possibly acetylene polymers as well as complex tholins (dark-reddish-brown, tarry, heteropolymeric, organic solids; Khare et al., 1986; McDonald et al., 1996). Ammonia would reduce the radar albedo but not the visual albedo (Lorenz, 1998), whereas the other contaminants would do both. (In the case of the polar organics, lowering of the visual albedo would be furthered as UV photons or charged particle radiation act on the material.)

Let $K = K_r + iK_i$ be a material's complex dielectric constant and define the loss tangent as $\tan\delta = K_i/K_r$. Then the $1/e$ one-way power absorption length can be written

$$L_{abs} = (\lambda/4\pi)\{(K_r/2)[(1+\tan^2\delta)^{1/2}-1]\}^{1/2}, \quad (6)$$

where λ is wavelength. For sufficiently small $\tan\delta$, we can use the approximation

$$L_{abs} = \lambda/[2\pi(K_r)^{1/2}\tan\delta]. \quad (7)$$

At 13.78 GHz, pure water ice has $K_r = 3.1$ and $K_i = 10^{-6}$ (Thompson and Squyres, 1990) and hence an absorption length of about 100,000 wavelengths, orders of magnitude longer than for most non-water ice mineral assemblages expected on planetary surfaces (e.g., Olhoeft and Strangway, 1975). Terrestrial rocks and nonmetallic meteorites have K_r between 2 and 10, and $\tan\delta$ between ~0.001 and 0.2 with a typical value of ~0.04. Corresponding values of L_{abs} range from about λ to ~100λ. Extremely small concentrations of impurities can dramatically reduce the microwave transparency of water ice (e.g., Chyba et al., 1998, and references therein). L_{abs} will increase roughly in proportion to porosity, so we might expect porous regoliths of ice containing a percent or so of impurities to have L_{abs} between 10λ and 100λ.

Contamination of water ice by ammonia can increase the loss tangent and decrease the absorption length dramatically, by up to several orders of magnitude even for concentrations less than a percent (Lorenz and Shandera, 2001, and references therein). Could ammonia be an important factor in the satellites' radar albedos? There is little or no near-infrared spectroscopic evidence for ammonia in the Saturn system. Emery et al. (2005) interpreted a weak feature near 2.25 μm in their near-IR spectrum of the south pole of Enceladus as a possible signature of a stoichiometric water–ammonia ice, but it does not appear equatorward on Enceladus or on other saturnian satellites observed in the infrared. (Cruikshank et al. (2005) place an upper limit of about 0.5 weight percent of NH_3 in water ice as a hydrate or as frozen NH_4OH on any of the satellites.) Yet Titan's Ar/N_2 ratio strongly points to NH_3 or some other nitrogen-bearing compound more refractory than N_2 as the source of Titan's atmosphere. NH_3 is expected on cosmogonic grounds (Lewis, 1972; Pollack et al., 1976), and its incorporation in Enceladus would ease the problem of explaining resurfacing of that object (Squyres et al., 1983). To simultaneously account for its role in affecting the radar properties while being absent from near-infrared spectra requires postulating that ammonia is depleted from the very outermost layer (centimeters or less) to which near-infrared spectra are sensitive, while being preserved at depths to which the radar sounds. Because UV or charged-particle chemistry will rapidly destroy exposed ammonia, converting it to hydrazine and then nitrogen (Lanzerotti et al., 1984), this is a plausible hypothesis (see Section 7), but we emphasize that it does not constitute positive evidence for the presence of this oft-cited but elusive volatile.

Matsuoka et al. (1996) explored the dependence of the electrical properties of water ice on frequency from 5 to 39 GHz and on temperature from 190 to 270 K. Their results imply that K_i increases as frequency increases, so that the absorption length's proportionality to wavelength is slightly greater than in Eqs. (6) and (7). Also, at a given wavelength, L_{abs} is slightly longer where it is colder, that is, within surfaces that have higher optical albedos. Thus we would expect cleaner ice to allow more efficient volume scattering both because of the absence of lossy impurities and because the lower temperature increases water ice's transparency.

The enormous 2.2-cm radar albedos of Enceladus and Tethys probably require that at least the uppermost one to several decimeters of the surface be extremely clean water ice regolith that is structurally complex (i.e., mature) enough for there to be high-order multiple scattering within it. This is met in part by relatively recent/ongoing geologic activity and the resultant resurfacing by clean water ice.

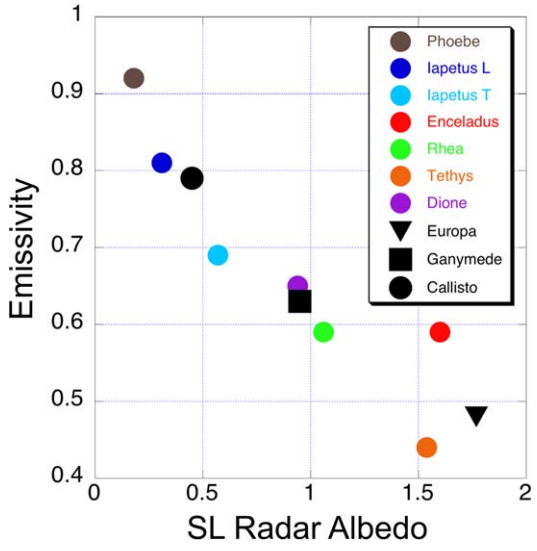

Fig. 5. Average emissivity vs average SL radar albedo. Emissivity is the ratio of disk brightness temperature $T_{\rm disk}$ to the equilibrium physical temperature, as inferred from the optical albedo; see Table 1. All emissivities and Saturn satellite radar albedos are 2.2-cm values. Galilean satellite albedos are 3.5-cm values from Ostro et al. (1992), and Galilean satellite emissivities are from de Pater et al. (1984).

Preliminary analysis of our Hyperion measurements indicates that despite an optical geometric albedo near the average value for Iapetus and spectrophotometric similarities to Iapetus (Buratti et al., 2005b; Denk et al., 2005), Hyperion's radar brightness may exceed those of all our other targets except Enceladus and Tethys (Table 1). Simulations by Dobrovolskis and Lissauer (2004) show that Hyperion reaccretes only ∼5% of its impact ejecta. They suggest that this low efficiency of reaccretion may help explain Hyperion's small size and rugged shape. Perhaps Hyperion's optical coloring is due to a thin layer of exogenously derived material that has never been worked into the icy regolith, which remains very clean and radar bright.

6. Phoebe's thermal penetration depth

The Phoebe inbound and outbound observations yielded nearly identical radar albedos but very different radiometric disk temperatures ($T_{\rm disk}$) of 93 and 75 K, respectively. The inbound observations were above the dawn terminator at latitude −22° and the outbound observations were about 5° sunward of the dusk terminator at about +27°.

The sensed temperature may be thought of as the weighted combination of three temperature distributions. First, and with the greatest variation across the surface, is the instantaneous radiative equilibrium temperature, varying only with the angular distance from the subsolar point. Beneath this, there is a temperature distribution that reflects the diurnally averaged insolation: peak temperatures are at the subsolar latitude and fall off north and south. At deeper levels still, the temperatures reflect the annually averaged insolation, being symmetric about the equator. The depth boundaries between these idealized distributions (which in reality are diffused together and thus any observation yields a weighted sum of the three) are roughly the penetration depths of the diurnal and seasonal thermal waves.

To first order, the thermal penetration depth can be written

$$L_{\rm thermal} = (\kappa\tau)^{1/2}. \tag{8}$$

Here τ is the time scale (here either Phoebe's rotation period of 9.25 h or Saturn's orbit period of 29 y) and the thermal diffusivity $\kappa = k/(\rho C)$, where k is the thermal conductivity, ρ is the density, and C is the heat capacity. Plausible thermal diffusivities for Solar System regoliths range from 10^{-6} m^2 s^{-1} for solid ice or rock to 10^{-7} m^2 s^{-1} for porous regolith. Thus the diurnal penetration depth is probably between 0.05 and 0.2 m, while the seasonal penetration depth is between 9 and 30 m.

If the microwave radiation were absorbed within ∼0.1 m of the surface, we would expect a large difference in the inbound and outbound values of $T_{\rm disk}$ due to the diurnal temperature cycle. We see such a difference, but its sense is opposite to that of Phoebe's actual diurnal cycle (dusk temperatures warmer than dawn). On the other hand, if microwaves penetrate deeply (>20 m) into Phoebe's surface, almost no difference would be seen in the two radiometric observations, since the annually averaged insolations (given Phoebe's obliquity of 17°) at −22° and +27° are within about 10% of each other, corresponding to equilibrium temperatures within about 3 K of each other.

We conclude that the middle distribution (for the diurnally averaged temperature) explains most of the observed inbound/outbound difference in $T_{\rm disk}$. With the subsolar point during the observation at −12°, the disk-averaged diurnal-average temperature is expected to be about 29% cooler as seen from our outbound nadir latitude (+27°) than from our inbound nadir latitude (−22°). That our sensed difference (with outbound $T_{\rm disk}$ ∼ 20% cooler than inbound $T_{\rm disk}$) is smaller probably reflects the dilution of the diurnal-averaged temperature distribution by emissions that are deep (with small temperature contrasts), or shallow (with opposite temperature contrasts), or both. Thus the radiometric temperatures imply that Phoebe's microwave emission contains contributions from decimeter-to-decameter depths, consistent with a significant volume-scattering contribution to Phoebe's radar albedo. A joint study of the Phoebe surface temperatures sensed by RADAR and by Cassini's Composite Infrared Spectrometer (Spencer et al., 2004; Pearl et al., 2004), taking advantage of the CIRS instrument's fine spatial resolution and accounting for Phoebe's complex topography, could yield further insights.

7. Iapetus: wavelength dependence

For Iapetus, our average 2.2-cm TP albedo is several times larger than the average 13-cm value. This strong drop in radar albedo from 2.2 to 13 cm is reminiscent of the 13-to-70-cm drop in the radar albedos of the icy Galilean satellites (Black et al., 2001a), which Black et al. (2001b) interpret as due to a decrease in the number density of scatterers with increasing size in the decimeter-to-meter size regime. However, the icy Galilean satellites' 3.5- and 13-cm albedos are virtually indistinguishable (Ostro et al., 1992), so there is "self similarity" in the structure responsible for scattering in this smaller size regime.

The interplanetary flux of micrometer-to-decimeter sized meteoroids is similar at the heliocentric distances of Jupiter and Saturn, and within an order of magnitude of the flux at 1 AU. This flux will lead to faster regolith maturation (in terms of grain size and porosity distributions) at small spatial scales than at larger scales. Thus, at centimeter-to-decimeter scales, we have no reason to expect the structural character of the top few meters of Saturn's icy satellites to differ significantly from that of Europa, Ganymede, or Callisto (or for that matter from that of the Moon; Ostro and Shoemaker, 1990, and references therein).

Similarly, we expect that the *purely structural* requirements for a regolith to be an efficient volume scatterer at centimeter-to-decimeter wavelengths are easily met, so that if structure were a sufficient condition, relatively ancient surfaces (Callisto, Phoebe) would be just as radar bright as relatively young surfaces (Europa, Enceladus). Once those structural requirements for efficient volume back scattering are attained, additional exposure to the meteoroid flux will not alter the centimeter-to-decimeter radar signature. Hence, for such short radar wavelengths, composition probably trumps structure as the source of radar albedo variation.

In this context, we conjecture that Iapetus' 2.2-to-13-cm albedo drop is caused by the increasing presence of ammonia with depth below the surface. As noted above, Lanzerotti et al. (1984) argue that a combination of ion erosion and micrometeoroid gardening should deplete ammonia from the surfaces of Saturn's icy satellites. Given the hypersensitivity of water ice's absorption length to ammonia concentration, an increase in ammonia with depth could allow efficient 2.2-cm scattering from within the top one to several decimeters while attenuating 13-cm echoes, which would require a six-fold thicker scattering layer. If so, we would expect each of the icy satellites' average radar albedos to be higher at 2.2 cm than at 13 cm, as is the case so far with Rhea as well as Iapetus.

Lanzerotti et al. (1984) suggest that ammonia removal on Enceladus could be of order tens of centimeters (erosion by protons) to tens of meters (erosion by oxygen ions) per billion years. Volcanic activity probably driven by subsurface ammonia is resurfacing Enceladus and feeding material into the E-ring, while sputtering of surface and ring particles produces a torus of neutral molecules that are ionized, maintaining the plasma in Saturn's inner magnetosphere (Johnson, 1996). The plasma's sputtering rates for condensed H_2O (Johnson, 1990) increase from Mimas away from Saturn, peak at Dione and then decrease slightly for Rhea. Ammonia depletion by magnetospheric ion bombardment presumably is much less effective for Hyperion, Iapetus, and Phoebe, which are subject to a different plasma environment than those inside Titan's orbit and within the magnetopause (Delitsky and Lane, 2002). At the outer satellites' distances from Saturn, protons are the dominant species, whereas in the inner part of the system the plasma consists primarily of a corotating comet-like mix of water derived ions (Young et al., 2005).

As noted by Lanzerotti et al., ammonia and water have vastly different vapor pressures, so the vaporization and fractionation produced by micrometeoroid impact would tend to deplete surfaces of NH_3 preferentially. Gravitational focusing enhances the meteoroid flux closer to Saturn (e.g., Morfill et al., 1983), so both this process and ion sputtering may be much less effective on Iapetus than on the inner satellites. If so, we would expect that compared to Iapetus, those objects would exhibit higher radar albedos (in addition to less severe 13-to-2.2-cm albedo dependence), as is seen.

8. Iapetus' hemispheric dichotomy

Our two Iapetus tracks were centered at (66° W, +39°) on the leading side and at (296° W, +46°) on the trailing side. Iapetus' 2.2-cm albedo is dramatically higher for our trailing-side observation than for our leading-side observation, requiring that to depths of at least one to several decimeters, the water ice is significantly "dirtier" on the leading side than the trailing side. By contrast, at 13 cm, little hemispheric asymmetry was seen by Black et al. (2004). We interpret this pair of results to mean that the leading-side contamination responsible for attenuating our 2.2-cm echo is effectively not really "seen" at all at 13 cm, either because it is intrinsically shallow and/or because the 13-cm scattering is already so attenuated by ammonia underneath our hypothesized ammonia-free layer that further absorption by the optically dark contaminant is minor.

Whereas our trailing-side view included part of the dark terrain near the periphery of the disk, our leading-side view was within about 20° of the northern limit of the dark terrain, so a significant fraction of the disk encompassed bright terrain. Therefore, the actual 2.2-cm albedo difference between the dark and bright terrains may well be much more severe than our numbers indicate.

What causes the disparity between the leading and trailing sides' 2.2-cm radar albedos? Iapetus is outside the Saturn magnetosphere, so one would not expect a hemispheric dichotomy in sputtering rates. Instead, differential cratering rates may be a factor; for example, Korycansky and Zahnle (2005) calculate an apex:antapex cratering asymmetry of 4:1 for Titan. For Iapetus the impact ratio would be much smaller, but not unity.

Thus it seems more appropriate to discuss the radar disparity in the context of possible surficial contamination of the leading side by the material that has optically darkened it. This idea is consistent with the contention (e.g., Buratti and Mosher, 1995) that the leading side contaminant is ballistically emplaced material originally ejected from Phoebe, Titan, and/or much smaller Saturn satellites, and that this process is a long-term one. Groundbased spectra of Iapetus' optically dark side has been modeled with a mixture of water ice, amorphous carbon, and tholin (Owen et al., 2001), and spectra obtained by Cassini's Visual and Infrared Mapping Spectrometer (VIMS) for the dark side has been modeled with a combination of tholin, poly-HCN, and small amounts of water ice and Fe_2O_3 (Buratti et al., 2005a, 2005b). Fe_2O_3 (hematite) is a semiconductor (Bosman and van Daal, 1970; Olhoeft, 1979) and easily could undermine the transparency of water ice. For hematite and other naturally occurring semiconductors like troilite (FeS; Egan and Hilgeman, 1977), the electrical properties are dispersive, and the loss tangent of rocks or regolith containing them can depend on frequency as well as on the material's physical state and

chemical purity (Ulaby et al., 1988). For pure hematite, 2.2-to-13-cm values for L_{abs} are very small fractions of a wavelength (Heggy, 2005, and personal comm.). (Because of their novel electromagnetic properties, iron oxide composites (ferrites) are used industrially as microwave absorbers, for example, in the seals of microwave ovens (Matsumoto et al., 2002).)

Although microwave absorption loss in hydrocarbons was not deemed consequential by Thompson and Squyres (1990), measurements of tholins at 2.2 cm by Rodriguez et al. (2003) yield typical values of $(K_r, K_i) = (2.2, 0.05)$, corresponding to $\tan\delta = 0.023$ and L_{abs} of a decimeter. Thus tholins may be the primary contaminant responsible for the dark terrain's low radar and optical albedos, and may also play a role in these properties elsewhere in the Saturn system.

9. Conclusion

Fortuitously, Cassini radar scatterometry appears to offer an indicator of water ice purity throughout the satellite system. Comparison of 2.2- and 13-cm albedos can help us assess regolith maturity, the systematics of ammonia depletion in near-surface layers, and contamination by optically dark and radar-absorbing materials.

Several of our flybys have included scatterometry with the beamwidth smaller than the target's disk and with the beam pointed at several different off-center positions. Analysis of these observations is underway, and should elucidate the degree to which satellite surfaces have uniform radar albedos. We also took data with a waveform that might allow resolution of echoes in range as well as in Doppler frequency, which would help to identify smaller-scale heterogeneities. Observations scheduled for flybys between now and 2008 will triple Cassini's radar coverage of the icy satellites' surfaces.

Acknowledgments

Part of this research was conducted at the Jet Propulsion Laboratory (JPL), California Institute of Technology, under contract with the National Aeronautics and Space Administration (NASA). We thank two anonymous referees for their careful critiques of our paper, Peter Thomas and the ISS Team for the use of their Phoebe shape model, Andre Yavrouian for discussions of organic chemistry, Essam Heggy for discussions of electrical properties, Bonnie Buratti for discussions of optical properties, and scientists on the other Cassini teams for valuable interactions. We gratefully acknowledge those who designed, developed and operate the Cassini/Huygens mission, which is a joint endeavor of NASA, the European Space Agency (ESA), and the Italian Space Agency (ASI) and is managed by JPL/Caltech under a contract with NASA.

References

Baars, J.W.M., Genzel, R., Pauliny-Toth, I.I., Witzel, A., 1977. The absolute spectrum of CAS A: An accurate flux density scale and a set of secondary calibrators. Astron. Astrophys. 61, 99–106.

Black, G.J., 1997. Chaotic rotation of Hyperion and modeling the radar properties of the icy Galilean satellites as a coherent backscatter effect. Ph.D. thesis, Cornell University.

Black, G., Campbell, D., 2004. Rhea's surface: Ice properties measured by radar. Bull. Am. Astron. Soc. 36, 1123.

Black, G.J., Campbell, D.B., Ostro, S.J., 2001a. Icy Galilean satellites: 70 cm radar results from Arecibo. Icarus 151, 160–166.

Black, G.J., Campbell, D.B., Nicholson, P.D., 2001b. Icy Galilean satellites: Modeling radar reflectivities as a coherent backscatter effect. Icarus 151, 167–180.

Black, G.J., Campbell, D.B., Carter, L.M., Ostro, S.J., 2004. Radar detection of Iapetus. Science 304, 553.

Bosman, A.J., van Daal, H.J., 1970. Small-polaron versus band conduction in some transition-metal oxides. Adv. Phys. 19, 1–117.

Buratti, B.J., Mosher, J.A., 1995. The dark side of Iapetus: Additional evidence for an exogenous origin. Icarus 115, 219–227.

Buratti, B.J., Cruikshank, D.P., Brown, R.H., Clark, R.N., Bauer, J.M., Jaumann, R., McCord, T.B., Simonelli, D.P., Hibbitts, C.A., Hansen, G.B., Owen, T.C., Baines, K.H., Bellucci, G., Bibring, J.-P., Capaccioni, F., Cerroni, P., Coradini, A., Drossart, P., Formisano, V., Langevin, Y., Matson, D.L., Mennella, V., Nelson, R.M., Nicholson, P.D., Sicardy, B., Sotin, C., Roush, T.L., Soderlund, K., Muradyan, A., 2005a. Cassini Visual and Infrared Mapping Spectrometer observations of Iapetus: Detection of CO_2. Astrophys. J. 622, L149–L152.

Buratti, B.J., Hicks, M.D., Davies, A., 2005b. Spectrophotometry of the small satellites of Saturn and their relationship to Iapetus, Phoebe, and Hyperion. Icarus 175, 490–495.

Chyba, C.F., Ostro, S.J., Edwards, B.C., 1998. Radar detectability of a subsurface ocean on Europa. Icarus 134, 292–302.

Cruikshank, D.P., Owen, T.C., Dalle Ore, C., Geballe, T.R., Roush, T.L., de Bergh, C., Sandford, S.A., Poulet, F., Benedix, G.K., Emery, J.P., 2005. A spectroscopic study of the surfaces of Saturn's large satellites: H_2O ice, tholins, and minor constituents. Icarus 175, 268–283.

Delitsky, M.L., Lane, A.L., 2002. Saturn's inner satellites: Ice chemistry and magnetosphere effects. J. Geophys. Res. 107 (E11), doi:10.1029/2002JE001855. 5093.

Denk, T., Neukum, G., Roatsch, Th., Burns, J.A., Helfenstein, P., Porco, C.C., and Cassini ISS Team, 2005. Surface colors of Iapetus and Hyperion as derived from Cassini ISS data, and implications for the global albedo dichotomy origin. Bull. Am. Astron. Soc. 37, 706.

de Pater, I., Lissauer, J.J., 2001. Planetary Sciences. Cambridge Univ. Press, Cambridge.

de Pater, I., Brown, R.A., Dickel, J.R., 1984. VLA observations of the Galilean satellites. Icarus 57, 93–101.

Dobrovolskis, A.J., Lissauer, J., 2004. The fate of ejecta from Hyperion. Icarus 169, 462–473.

Egan, W.G., Hilgeman, T., 1977. The rings of Saturn: A frost-coated semiconductor? Icarus 30, 413–421.

Elachi, C., Allison, M.D., Borgarelli, L., Encrenaz, P., Im, E., Janssen, M.A., Johnson, W.T.K., Kirk, R.L., Lorenz, R.D., Lunine, J.I., Muhleman, D.O., Ostro, S.J., Picardi, G., Posa, F., Rapley, C.G., Roth, L.E., Seu, R., Soderblom, L.A., Vetrella, S., Wall, S.D., Wood, C.A., Zebker, H.A., 2005a. RADAR: The Cassini Titan Radar Mapper. Space Sci. Rev. 117, 71–110.

Elachi, C., Wall, S., Allison, M., Anderson, Y., Boehmer, R., Callahan, P., Encrenaz, P., Flamini, E., Franceschetti, G., Gim, Y., Hamilton, G., Hensley, S., Janssen, M., Johnson, W., Kelleher, K., Kirk, R., Lopes, R., Lorenz, R., Lunine, J., Muhleman, D., Ostro, S., Paganelli, F., Picardi, G., Posa, F., Roth, L., Seu, R., Shaffer, S., Soderblom, L., Stiles, B., Stofan, E., Vetrella, S., West, R., Wood, C., Wye, L., Zebker, H., 2005b. Cassini radar views the surface of Titan. Science 308, 970–974.

Emery, J.P., Burr, D.M., Cruikshank, D.P., Brown, R.H., Dalton, J.B., 2005. Near-infrared (0.8–4.0 μm) spectroscopy of Mimas, Enceladus, Tethys, and Rhea. Astron. Astrophys. 435, 353–362.

Finney, D.J., 1964. Statistical Method in Biological Assay, second ed. Hafner, New York, p. 24.

Garvin, J.B., Head, J.W., Pettengill, G.H., Zisk, S.H., 1985. Venus global radar reflectivity and correlations with elevation. J. Geophys. Res. 90, 6859–6871.

Hapke, B., 1989. Coherent backscatter: An explanation for the unusual radar properties of outer planet satellites. Bull. Am. Astron. Soc. 21, 984.

Harmon, J.K., Nolan, M.C., Ostro, S.J., Campbell, D.B., 2004. Radar studies of comet nuclei and grain comae. In: Festou, M., Keller, U., Weaver, H. (Eds.), Comets II. Univ. of Arizona Press, Tucson, pp. 265–279.

Heggy, E., 2005. Loss tangent map of the martian surface: A frequency dependent model for the near equatorial regions. Lunar Planet. Sci. 36. Abstract 2109.

Janssen, M.A., Paganelli, F., Kirk, R., Lorenz, R.D., Lopes, R.M., and Cassini RADAR Team, 2005. Titan's surface properties from the Cassini RADAR radiometer. Bull. Am. Astron. Soc. 37, 739.

Johnson, R.E., 1990. Energetic Charged-Particle Interactions with Atmospheres and Surfaces. Springer-Verlag, Berlin, pp. 146–157.

Johnson, R.E., 1996. Sputtering of ices in the outer Solar System. Rev. Mod. Phys. 68, 305–312.

Khare, B., Sagan, C., Ogino, H., Nagy, B., Er, C., Schram, K.H., Arakawa, E.T., 1986. Amino acids derived from Titan tholins. Icarus 68, 176–184.

Korycansky, D.G., Zahnle, K.J., 2005. Modeling crater populations on Venus and Titan. Planet. Space Sci. 53, 695–710.

Küppers, M., Bertini, I., Fornasier, S., Gutierrez, P.J., Hviid, S.F., Jorda, L., Keller, H.U., Knollenberg, J., Koschny, D., Kramm, R., Lara, L.-M., Sierks, H., Thomas, N., Barbieri, C., Lamy, P., Rickman, H., Rodrigo, R., and OSIRIS Team, 2005. A large dust/ice ratio in the nucleus of Comet 9P/Tempel 1. Nature 437, 987–990.

Lanzerotti, L.J., Brown, W.L., Marcantonio, K.J., Johnson, R.E., 1984. Production of ammonia-depleted surface layers on the saturnian satellites by ion sputtering. Nature 312, 139–140.

Lewis, J., 1972. Low temperature condensation from the solar nebula. Icarus 16, 241–252.

Long, M.W., 1965. On the polarization and the wavelength dependence of sea echo. Trans. IEEE AP-14, 749–754.

Lorenz, R.D., 1998. Preliminary measurements of the cryogenic dielectric properties of water–ammonia ices: Application to radar observations of icy satellites. Icarus 136, 344–348.

Lorenz, R.D., Shandera, S.E., 2001. Physical properties of ammonia-rich ice: Application to Titan. Geophys. Res. Lett. 28, 215–218.

MacKintosh, F.C., John, S., 1989. Diffusing-wave spectroscopy and multiple scattering of light in correlated random media. Phys. Rev. B 40, 2383–2406.

Magri, C., Ostro, S.J., Rosema, K.D., Thomas, M.L., Mitchell, D.L., Campbell, D.B., Chandler, J.F., Shapiro, I.I., Giorgini, J.D., Yeomans, D.K., 1999. Main belt asteroids: Results of Arecibo and Goldstone radar observations of 37 objects during 1980–1995. Icarus 140, 379–407.

Matsumoto, K., Yuusuke, K., Osamu, H., 2002. An analysis of a door seal structure of a microwave oven with an inserted sheet-type lossy material using FDTD method. Electron. Commun. Jpn. Part I Commun. 85, 13–20.

Matsuoka, T., Fujita, S., Mae, S., 1996. Effect of temperature on dielectric properties of ice in the range 5–39 GHz. J. Appl. Phys. 80, 5884–5890.

McDonald, G.D., Whited, L.J., DeRuiter, C., Khare, B.N., Patnaik, A., Sagan, C., 1996. Production and chemical analysis of cometary ice tholins. Icarus 122, 107–117.

Morfill, G.E., Fechtig, H., Grun, E., Goertz, C.K., 1983. Some consequences of meteoroid impacts on Saturn's rings. Icarus 55, 439–447.

Morrison, D., Owen, T., Soderblom, L., 1986. The satellites of Saturn. In: Burns, J.A., Matthews, M.S. (Eds.), Satellites. Univ. of Arizona Press, Tucson, pp. 764–801.

Olhoeft, G., 1979. Tables of Room Temperature Electrical Properties for Selected Rocks and Minerals with Dielectric Permittivity Statistics. U.S. Geological Survey Open File Report 79-993.

Olhoeft, G.R., Strangway, D.W., 1975. Dielectric properties of the first 100 meters of the Moon. Earth Planet. Sci. Lett. 24, 394–404.

Ostro, S.J., 1993. Planetary radar astronomy. Rev. Mod. Phys. 65, 1235–1279.

Ostro, S.J., Shoemaker, E.M., 1990. The extraordinary radar echoes from Europa, Ganymede, and Callisto: A geological perspective. Icarus 85, 335–345.

Ostro, S.J., Campbell, D.B., Pettengill, G.H., Shapiro, I.I., 1980. Radar observations of the icy Galilean satellites. Icarus 44, 431–440.

Ostro, S.J., Campbell, D.B., Shapiro, I.I., 1985. Main belt asteroids: Dual-polarization radar observations. Science 229, 442–446.

Ostro, S.J., Campbell, D.B., Simpson, R.A., Hudson, R.S., Chandler, J.F., Rosema, K.D., Shapiro, I.I., Standish, E.M., Winkler, R., Yeomans, D.K., Velez, R., Goldstein, R.M., 1992. Europa, Ganymede, and Callisto: New radar results from Arecibo and Goldstone. J. Geophys. Res. 97, 18227–18244.

Owen, T.C., Cruikshank, D.P., Dalle Ore, C.M., Geballe, T.R., Roush, T.L., de Bergh, C., Meier, R., Pendleton, Y.J., Khare, B.N., 2001. Decoding the domino: The dark side of Iapetus. Icarus 149, 160–172.

Pearl, J.C., Spencer, J., Segura, M., 2004. Cassini CIRS observations of Phoebe's long-wavelength thermal emission. Bull. Am. Astron. Soc. 36, 1071.

Peters, K.J., 1992. The coherent backscatter effect: A vector formulation accounting for polarization and absorption effects and small or large scatterers. Phys. Rev. B 46, 801–812.

Pettengill, G.H., Ford, P.G., Chapman, B.D., 1988. Venus: Surface electromagnetic properties. J. Geophys. Res. 93, 14881–14892.

Pettengill, G.H., Ford, P.G., Wilt, R.J., 1992. Venus surface radiothermal emission as observed by Magellan. J. Geophys. Res. 97, 13091–13102.

Pollack, J.B., Grossman, A.S., Moore, R., Graboske Jr., H.R., 1976. The formation of Saturn's contraction history. Icarus 29, 35–48.

Porco, C.C., Baker, E., Barbara, J., Beurle, K., Brahic, A., Burns, J.A., Charnoz, S., Cooper, N., Dawson, D.D., Del Genio, A.D., Denk, T., Dones, L., Dyudina, U., Evans, M.W., Giese, B., Grazier, K., Helfenstein, P., Ingersoll, A.P., Jacobson, R.A., Johnson, T.V., McEwen, A., Murray, C.D., Neukum, G., Owen, W.M., Perry, J., Roatsch, T., Spitale, J., Squyres, S., Thomas, P.C., Tiscareno, M., Turtle, E., Vasavada, A.R., Veverka, J., Wagner, R., West, R., 2005. Cassini imaging science: Initial results on Phoebe and Iapetus. Science 307, 1237–1242.

Rodriguez, S., Paillou, P., Dobrijevic, M., Ruffié, G., Coll, P., Bernard, J.M., Encrenaz, P., 2003. Impact of aerosols present in Titan's atmosphere on the CASSINI radar experiment. Icarus 164, 213–227.

Spencer, J.R., Pearl, J.C., Segura, M., and Cassini CIRS Team, 2004. Cassini CIRS observations of Phoebe's 9–17 micron thermal emission. Bull. Am. Astron. Soc. 36, 1071.

Squyres, S.W., Reynolds, R.T., Cassen, P.T., Peale, S.J., 1983. The evolution of Enceladus. Icarus 53, 319–331.

Thompson, W.R., Squyres, S.W., 1990. Titan and other icy satellites: Dielectric properties of constituent materials and implications for radar sounding. Icarus 86, 336–354.

Ulaby, F.T., Bengal, T.H., East, J.R., Dobson, M.C. Garvin, J.B., Evans, D.L., 1988. Microwave dielectric spectrum of rocks. Radiation Lab. Tech. Rep. No. 023817-1-T. Dept. of Elect. Eng. and Computer Sci., Univ. of Michigan, Ann Arbor.

Veverka, J., Thomas, P., Johnson, T.V., Matson, D., Housen, K., 1986. The physical characteristics of satellite surfaces. In: Burns, J.A., Matthews, M.S. (Eds.), Satellites. Univ. of Arizona Press, Tucson, pp. 342–402.

Young, D.T., Berthelier, J.-J., Blanc, M., Burch, J.L., Bolton, S., Coates, A.J., Crary, F.J., Goldstein, R., Grande, M., Hill, T.W., Johnson, R.E., Baragiola, R.A., Kelha, V., McComas, D.J., Mursula, K., Sittler, E.C., Svenes, K.R., Szeg Barraclough, B.L., Bebesi, Z., Delapp, D., Dunlop, M.W., Gosling, J.T., Furman, J.D., Gilbert, L.K., Glenn, D., Holmlund, C., Illiano, J.-M., Lewis, G.R., Linder, D.R., Maurice, S., McAndrews, H.J., Narheim, B.T., Pallier, E., Reisenfeld, D., Rymer, A.M., Smith, H.T., Tokar, R.L., Vilppola, J., Zinsmeyer, C., 2005. Composition and dynamics of plasma in Saturn's magnetosphere. Science 307, 1262–1266.